Fuel Pellet and Rod Thermal Analysis

K M Zaheen Nasir

March 2024

1   Introduction

Recent undertakings in the nuclear power engineering community for increasing the life of LWR reactors and their constituents necessitate critical analysis of the prevalent fuel types in terms of their longevity, economy, performance at high burn-up, and temperature. Consequently, thermal analysis of LWR fuel is an important stepping stone for analyzing the critical thermo-mechanical performance of the fuel and its interaction with the surroundings. This is primarily because microstructure and material properties inside the fuel change as a function of temperature with time. Therefore, this project performs a thermal analysis of a UO_2 fuel pellet. The axial variation of the temperature field is also simulated for a single fuel rod.

Both the studies were performed in an axisymmetric manner in RZ coordinate. The given pellet geometry is shown in Figure 1. The fuel rod has similar dimensions for fuel, gap, and clad as the pellet except for the length, which is taken as 1 m. In the case of the pellet, both steady and transient thermal analyses have been performed for constant and temperature-dependent thermal conductivity of fuel and gap. Cladding thermal conductivity was taken as constant in all cases. For the fuel rod, only steady-state thermal analysis was performed for axially varying heat generation rate and coolant temperature with temperature-dependent thermal conductivity. Table 1 provides the material-specific thermal and flow parameters considered for these analyses.

2   Meshing

2.1   Pellet Geometry

The given geometry was meshed using the **GeneratedMeshGenerator** moose object. For the steady state analyses, we adopted a 1000 x 1000 elements mesh initially along R and Z directions respectively. Afterward, a convergence study showed that similar results can be achieved through a more coarse mesh of 125 x 125 elements within 1.5% error. Therefore, a mesh of 125 x 125 was used for the sake of alacrity in moving forward. Although a good FEM analysis requires
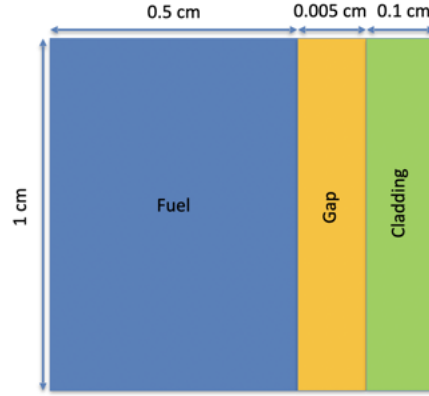
Figure 1: Pellet Geometry in RZ Coordinate (Axisymmetic 2D).

a balanced aspect ratio for each element's dimensions, the same number of elements in each dimension were used for this simple geometry without increasing the element number in Z direction. Moose object **SubdomainBoundingBox-Generator** were used to further subdivide the domain into three blocks representing fuel, gap, and cladding. Figure 2 shows the subdivisions of the problem domain. An element number of 125 is chosen in the R direction so that the element size (0.00484 cm) remains smaller than the gap width and the mesh object can easily recognize the gap block. However, any element size smaller than the gap size would've also worked. Similarly, we maintained the same number of elements for transient analyses as well.
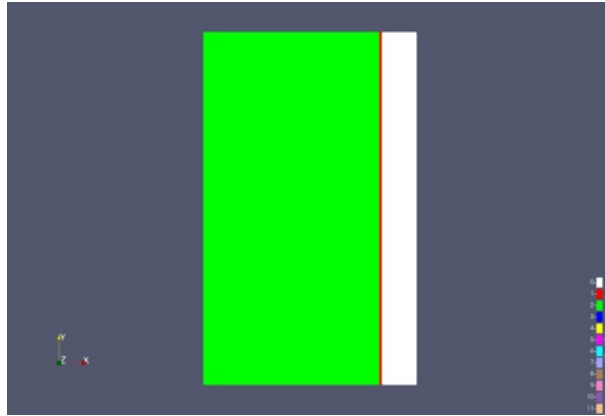

Figure 2: Mesh blocks representing fuel(Green), gap(red), cladding(white).

Quantity	Symbol	Value/Function
Outer Cladding Temperature	T_{CO}	550 K (pellet)
Fuel Thermal Conductivity Constant	K_F	0.03 $W/(cm * K)$
Fuel Thermal Conductivity Temp Dependent	K_{FT}	$K_{FT} = 1/(A + BT)$, $A = 3.8 + 200 * FIMA$, $B = 0.0217$
Gap Thermal Conductivity Constant	K_g	0.002556 $W/(cm * K)$
Gap Thermal Conductivity Temp Dependent	K_{gT}	$(16*10^{-6})*T^{0.79}$ $W/(cm*K)$
Cladding Thermal Conductivity	K_C	0.17 $W/(cm * K)$
LHR Steady	LHR/LHR^o	350 W/cm
LHR Transient	LHR	$250 * exp(-((t - 20)^2)/10) + 150$ W/cm
Coolant Flow rate	$\dot{m}$	0.05 $Kg/s - rod$ (a smaller value is taken to observe the effect of peak shifting)
Coolant Inlet Temperature	T_{cool}^{in}	500 K

Table 1: Material Specific Thermal and Flow Parameters for Fuel Pellet and Rod

2.2 Rod Geometry

We adopted a similar approach mentioned in section 2.2 to create the initial rod geometry and mesh. Thereafter, we used **SideSetsBetweenSubdomains-Generator** to generate and name the boundaries between fuel and gap as well as clad and gap respectively. To properly utilize the **GapHeatTransfer** under **ThermalContact** which calculates the heat transfer across an unmeshed gap, we also deleted the gap block using **BlockDeletionGenerator**. A slice of rod mesh blocks are shown in Figure 3. A convergence study was performed to determine the optimum number of elements for faster calculation with reasonable accuracy of axial variation. The study investigated starting from as little as 125 elements in either dimension up to 1500 elements. The impact of aspect ratio on the results was also investigated using **nx = 125 (R)** and **ny = 1500 (Z)** elements. No effect of aspect ratio was observed on the results. Also, a variation of only 3% was observed between the most refined and coarse mesh. Therefore, a mesh of 125 x 125 was finally adopted for these analyses. Table 2 lists the results of the convergence study for the axial variation of the temperature profile.
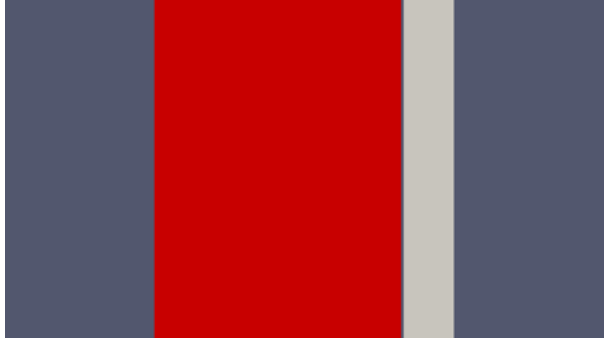
Figure 3: A slice of rod mesh blocks representing fuel (red) & cladding (gray) with unmeshed gap.

Mesh Size (x by y)	T(z=0m)	$T_{max}(z = 0.534m)$	T(z=1m)
125 x 125	790.128	1670.05	952.49
250 x 250	793	1680	957.549
500 x 500	792.42	1675.37	953.422
1000 x 1000	804.443	1722.14	966.73
1000 x 1500	804.46	1722.14	966.747
125 x 1500	791.485	1670.06	953.58

Table 2: Results of Convergence Study (Temperatures in K).

3 Kernels, Variables and Boundary Conditions

Thermal analyses of the fuel pellet and rod were done using the basic heat conduction equation as the governing equation over the respective problem domain. The strong and weak forms of the governing equations are presented below.

Strong Form:

$$\rho C_p \frac{\partial T}{\partial t} = \nabla.(k\nabla T) + Q \tag{1}$$

where ρ is the density, C_p is the specific heat, T represents the temperature profile of the fuel pellet and Q is the heat source.

Weak Form:

$$(\phi_i, \rho C_p \frac{\partial T}{\partial t}) + (\nabla \phi_i, k\nabla T) - \langle \phi_i, k\nabla T.\mathbf{n} \rangle + (\phi_i, Q) = 0 \tag{2}$$

where ϕ_i is the FEM weighting or trial function and $\mathbf{n}$ is the outward vector normal to the boundary. We obtain equation 2 (weak form) from the strong form of the heat conduction equation as per Galerkin formulation where the trial functions are the same as the FEM shape functions. Observing the weak form we

automatically understand that the MOOSE implementation requires three kernels for transient analysis for the terms shown within the parenthesis in Equation 2. The number of required kernels is reduced to two for steady-state analyses. We chose **HeatConduction**, **HeatSource**, and **SpecificHeatConduction-TimeDerivative** as the kernels of the said analysis. Standard formulations were used to convert **LHR** to heat source **Q** as an input to the **HeatSource** kernel.

The weak form also reveals the necessity of Neuman BC represented by the term within the angular brackets. On the other hand, Dirichlet BCs are directly implemented within the FEM shape function. Therefore, we apply Neuman BC of $\nabla T = 0$ on the left boundary representing the centerline of the fuel and T = 550 K on the right boundary as cladding outer temperature for the pellet thermal analyses. The scalar variable temperature is taken as the primary variable representing our required solution field.

For the fuel rod, the **LHR** and coolant temperature also vary axially. This necessitates the use of **FunctionDirichletBC** at the right boundary along with a function implementation within the **HeatSource**. The axial variation of the **LHR** and coolant temperature, T_{cool} can be captured by the following functions.

LHR:

$$LHR(z) = LHR^o cos[\frac{\pi}{2\gamma}(\frac{z}{z_o} - 1)] \tag{3}$$

where $z_o = 0.5m$ is the fuel midpoint.

T_{cool} :

$$T_{cool} = T_{cool}^{in} + \frac{2\gamma}{\pi}\frac{z_o.LHR^o}{\dot{m}.C_p}[sin\frac{\pi}{2\gamma} + sin\frac{\pi}{2\gamma}(\frac{z}{z_o} - 1)] \tag{4}$$

Functions were created using **ParsedFunction** object. We chose a value of 0.5 Kg/s-rod for the flow rate to observe the peak shifting of the fuel temperature. Although the value deviates from ideal scenario, it was needed to observe the peak shifting phenomenon for this smaller-than-ideal system. A γ value of 1.2 was used for the analysis considering extrapolation distance. The **GapHeatTransfer** under **ThermalContact** module was used to transfer the heat across the gap between fuel and cladding.

4   Choice of Materials

Our analyses were strictly kept within the LWR scenario. As a result, we chose UO_2 as our fuel material with Zircaloy-4 cladding. Helium is taken as the gas occupying the gap between fuel and cladding material for part one of this project. Naturally, we used water as a coolant for our simulations. Their material properties used in the simulations except for thermal conductivity (already given in table 1) are listed in table 3. These values were taken from the Lecture 3 slides of the Nuclear Fuel Performance course.

Properties	UO$_2$	He	Zircaloy-4	H$_2O$	Units
Density	10.98	$0.178 * 10^{-3}$	6.5	-	g/cm^3
Specific Heat	0.33	5.188	0.35	4200	$J/g - K$

Table 3: Material properties used for the Analyses.

5 Results

5.1 Pellet Radial Thermal Analysis

Considering helium in the gap we obtained the following analytical solution for the steady state.

$$\frac{\textbf{LHR}}{2\pi R_F} = \frac{350}{2\pi 0.5} = 111.408$$

Cladding inner temperature:

$$\therefore T_{CI} = T_{CO} + \frac{\textbf{LHR}.t_c}{2\pi R_F.K_C} = 550 + 111.408\frac{0.1}{0.17} = 615.534 \ K$$

Assuming $T_{CI} = T$ we have,

$$K_g = 16 * 10^{-6} * T^{0.79} = 0.002556 \ W/(cm.K)$$

$$h_{gap} = \frac{K_g}{t_g} = \frac{0.002556}{0.005} = 0.5112 \ W/(cm^2.K)$$

Fuel surface temperature:

$$\therefore T_S = T_{CI} + \frac{\textbf{LHR}}{2\pi R_F.h_{gap}} = 615.534 + \frac{111.408}{0.5112} = 833.46 \ K$$

Fuel centerline temperature:

$$\therefore T_o = T_S + \frac{\textbf{LHR}}{4\pi K_F} = 833.46 + \frac{350}{4\pi 0.03} = 1761.86 \ K$$

The results of the analyses along with the comparison of steady state solution with our analytical one are portrayed in table 4.

The contour plots and the spatial profiles of temperature along the radial direction of the fuel pellet including gap and cladding for both constant and temperature-dependent thermal conductivity of the steady state analyses are presented in figure 4 and 5 respectively.

Similar plots including the temporal profile of fuel centerline temperature up to 100 sec for both constant and temperature-dependent thermal conductivity are shown in figure 6 and 7 respectively.

Properties	Steady-Const. K	% Error	Steady-Temp. dep. K	Transient-Const. K	Transient-Temp. dep. K
Fuel centerline temp.(K)	1772.35	0.595	1642.95	1073.88	925.843
Fuel surface temp.(K)	844.943	1.378	818.943	676.407	675.377
Cladding inner temp.(K)	609.023	1.058	609.023	575.296	575.296
Cladding outer temp.(K)	550	0	550	550	550
Approach to steady state (sec)	-	-	-	50	45
Steady-state reached (sec)	-	-	-	85	72

Table 4: Analyses results and comparison with analytical solution.

Temperatures (K)	T(z=0.25m)	T(z=0.5m)	T(z=1m)
Fuel Centerline	1340.14	1665.04	950.91
Fuel Surface	747.71	833.94	728.03
Cladding Inner	573.99	623.46	650.96
Cladding Outer	525.51	564.72	629.45

Table 5: Radial temperature profiles at various heights along the rod.

5.2   Rod Axial Thermal Analysis

The radial temperature distribution of the fuel rod at z=0.25m, z=0.5m, and z=1m are presented in the table 5. The temperature profiles are shown in figure 8, 9, 10 respectively.

Due to the reduced flow rate, the peak fuel centerline temperature of 1670.06 K is observed at 53.5 cm. However, a peak fuel surface temperature of 842.761 is found at 60.8 cm as expected. The axial variations of temperatures are presented in figure 11 and 12 respectively.
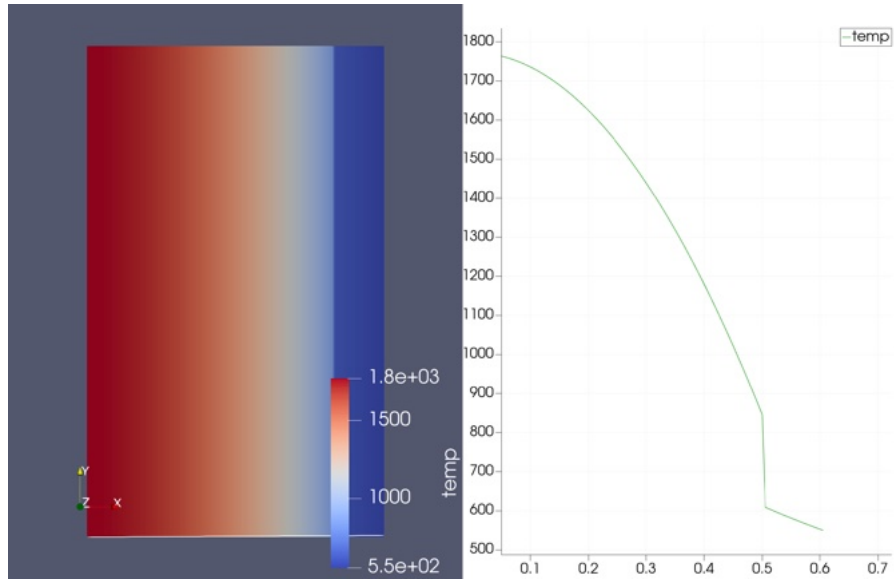
Figure 4: Contour and spatial temperature profile for constant thermal conductivity in steady state.
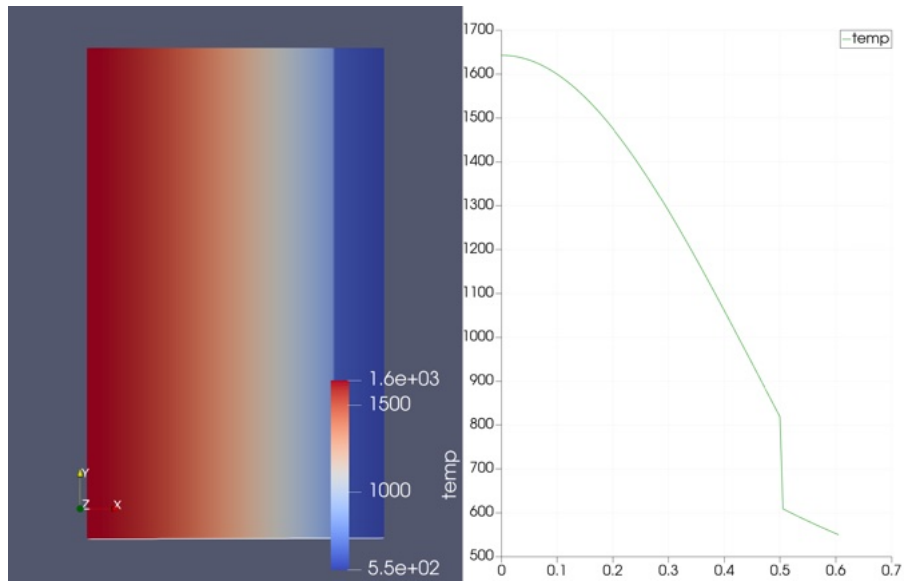

Figure 5: Contour and spatial temperature profile for temperature-dependent thermal conductivity in steady state.
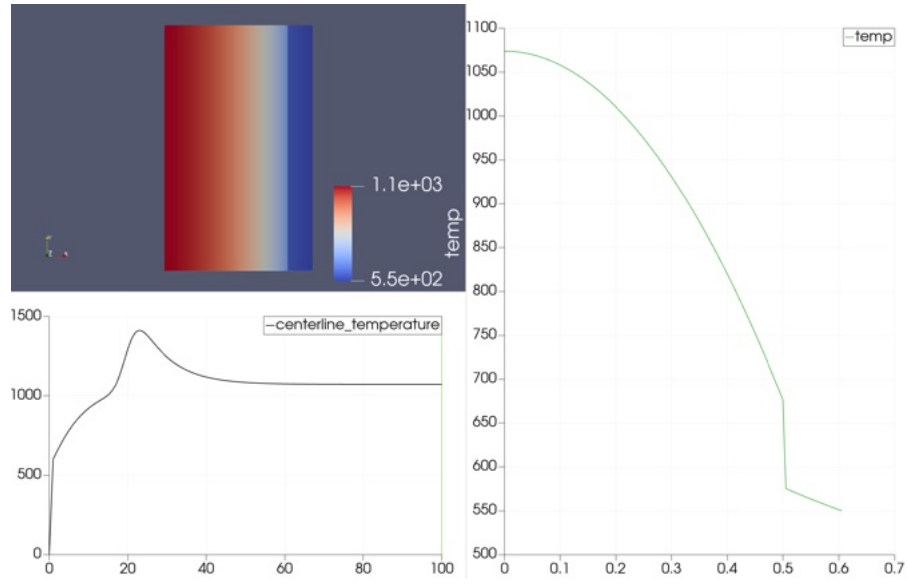
8

Figure 6: Contour, spatial temperature, and temporal fuel centerline temperature profile for constant thermal conductivity.
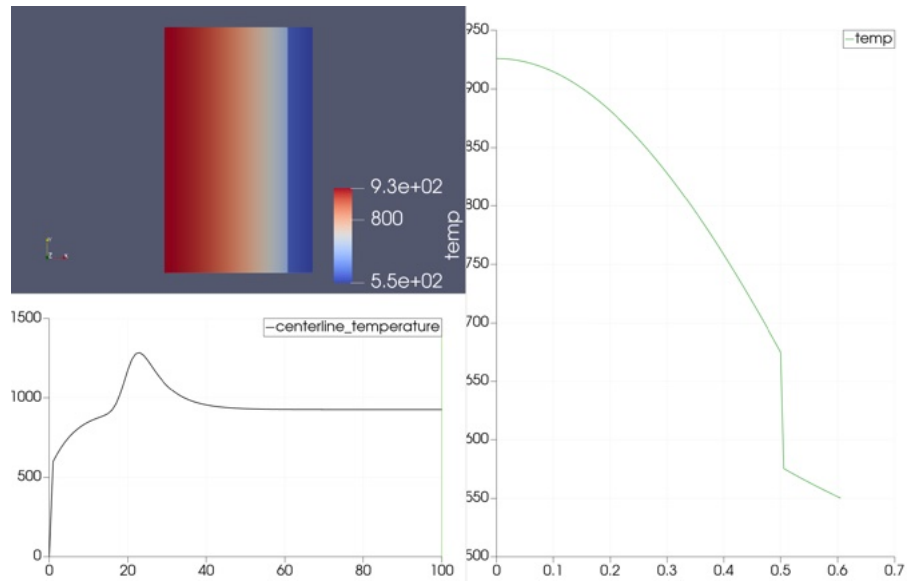

Figure 7: Contour, spatial temperature, and temporal fuel centerline temperature profile for temperature-dependent thermal conductivity.
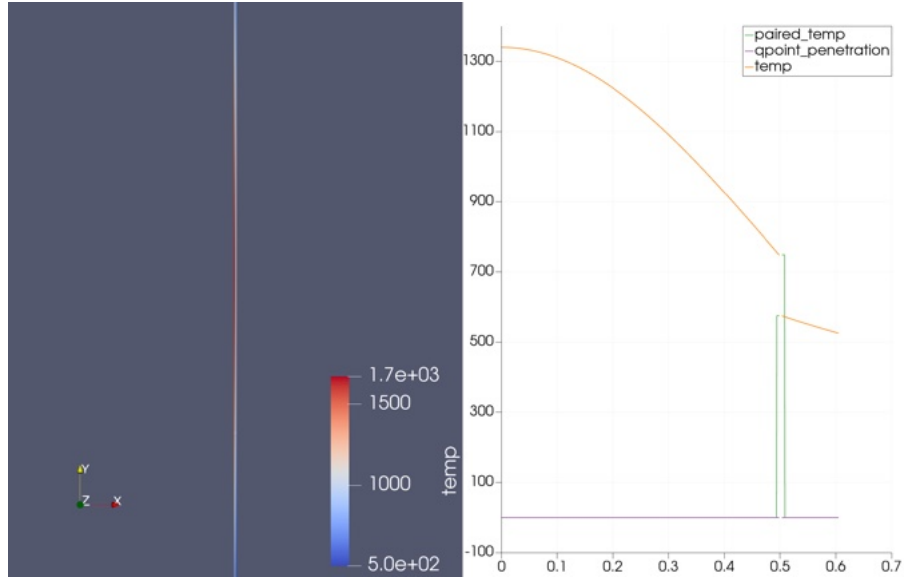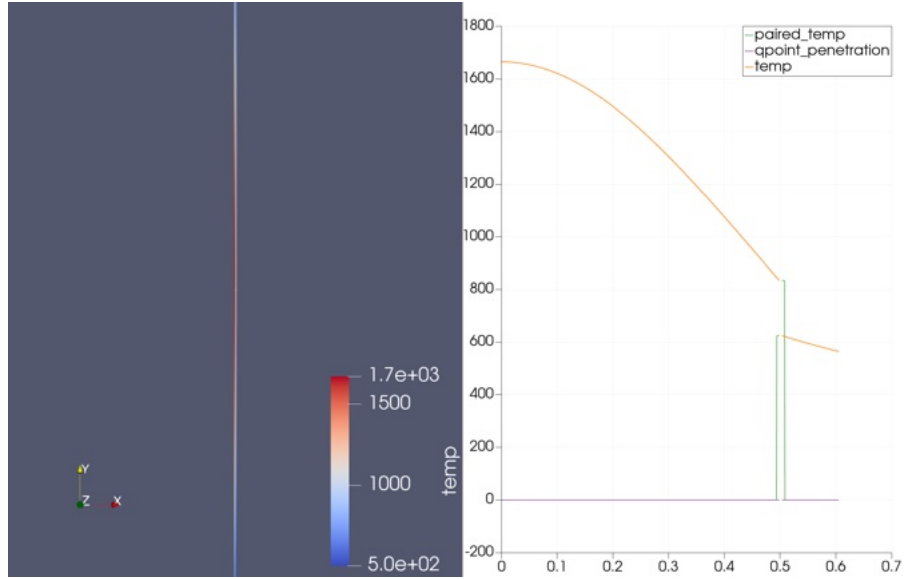
Figure 8: Temperature profile at z=0.25 m.

Figure 9: Temperature profile at z=0.50 m.

6   Discussion

In the case of pellet thermal analyses, comparison with the analytical solution for the steady state reveals negligible errors and points towards successful modeling
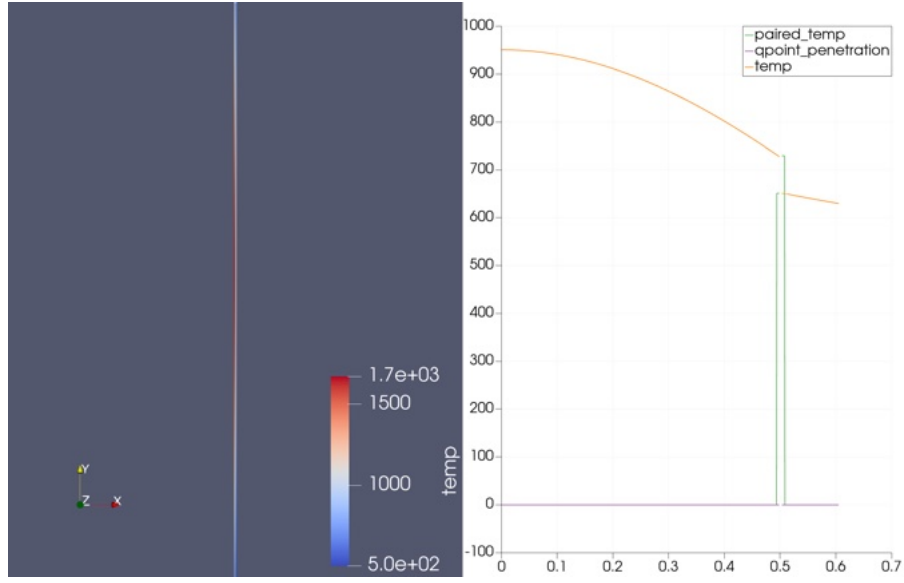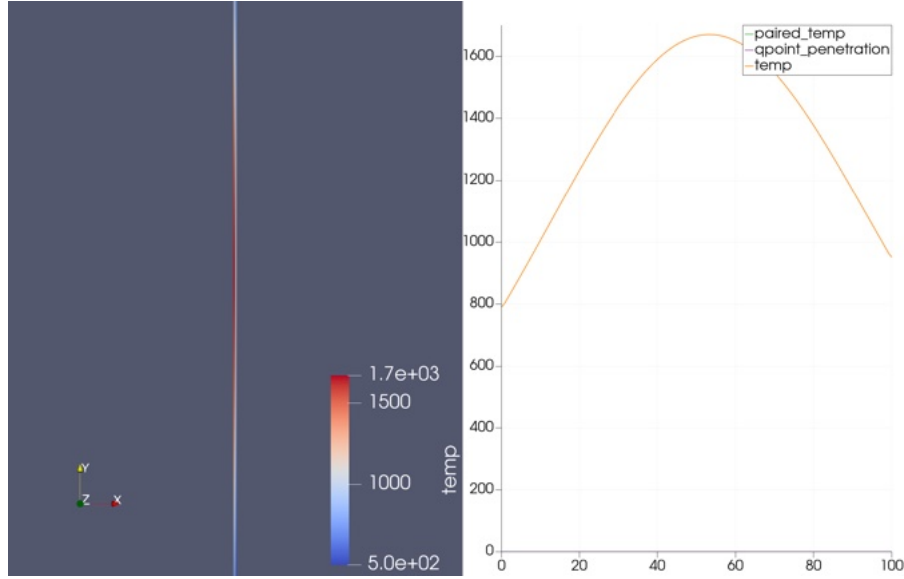
10

Figure 10: Temperature profile at z=1 m.

Figure 11: Axial profile of fuel centerline temperature.

of the fuel pellet temperature profile. According to our empirical dependence of thermal conductivity upon temperature as used in the simulation, fuel thermal conductivity decreases with increasing temperature while gap conductivity
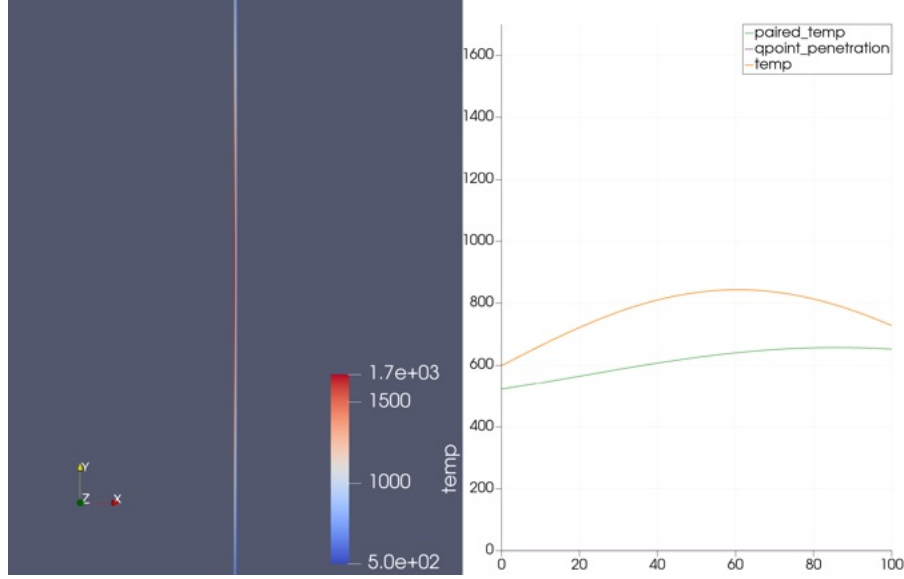
11

Figure 12: Axial profile of fuel surface temperature.

increases. However, as observed from our analysis, this had an overall effect of decreasing the fuel centerline temperature resulting in a lower thermal gradient across the fuel pellet compared to constant thermal conductivity. During the transient analyses, it was observed that the nonlinear solve fails to converge when the steady state is approached. This is because the nonlinear Newton-Raphson fails to find a suitable value for the scalar variable temperature that minimizes the residual beyond the set tolerance. The fact that the temperature doesn't deviate much due to the approaching steady state contributes to the inability of Newton-Raphson to minimize the residual beyond a certain value. This problem required a workaround by changing the nonlinear tolerances in the executioner block. We set **nl_rel_tol = 1e-10** and **nl_abs_tol = 1e-10** to obtain our transient solution. Transient analysis showed a peaking of the fuel centerline temperature at 23 sec reaching 1414.15 K and 1285.82 K for constant and temperature dependent thermal conductivity before reaching respective steady state. We used a post-processor object of **SideExtremeValue** to track the fuel centerline temperature.

For the rod thermal analyses, the temperature profiles obtained for various positions along the fuel rod are in reasonable agreement with the analytical solutions. In ideal cases, maximum fuel centerline temperature occurs around 60% of the fuel length. The maximum heat generation takes place at the midpoint of the fuel height. However, as the comparatively colder coolant moves upward through the channels between the fuel, it gradually becomes hotter by absorbing heat from the fuel rod. Which in turn shifts the peak centerline temperature towards the top. Nevertheless, our given system is significantly smaller than

the ideal to observe this peak at the said height. Therefore, with a reduced flow rate as mentioned earlier, we were able to observe the shifted peak at 53.5 cm for the fuel centerline temperature. The phenomenon of peak shifting is more pronounced in the case of the fuel surface temperature. We found the peak fuel surface temperature at 60.8 cm. The use of **GapHeatTransfer** resulted in insignificant variations in the temperature profile compared to the thermal analyses for the pellet.

7   Conclusion

Accomplishing this project has equipped us with hands-on knowledge for modeling the radial and axial variations of temperatures for the pellet and rod using MOOSE. Although MOOSE is a powerful modular and pluggable framework for performing a wide range of analyses, a thorough understanding of physics behind the problem and numerical schemes such as FEM, implicit time integration using Newton-Raphson or Preconditioned Jacobian Free Newton Krylov (PJFNK) etc in solving the problem is essential. Obtaining a transient solution by tweaking the tolerances that don't deviate from the expected behavior according to the physics of the problem domain is a testament to this requirement. Additionally, a grasp on versatile powerful modules and action systems like **GapHeatTransfer** under the **ThermalContact** will lead to simulations with a significant reduction of efforts. Eventually, these will allow us to perform any kind of large-scale analysis using MOOSE or any type of modeling tool similar to MOOSE.